Reactive Extrusion Strategies to Fabricate Magnetite–Polyethylene Nanocomposites with Enhanced Mechanical and Magnetic Hyperthermia Properties

Shu F. Situ, Jingshan Cao, Chuhang Chen, Eric C. Abenojar, João M. Maia,* Anna Cristina S. Samia*

Biofouling is a major problem in water filtration units, which leads to premature system failure. Conventional treatment methods involving the use of chemicals or high-pressure hydraulics exert mechanical strain on filter materials, leading to shortened service lifetimes. In this study, a novel magnetic polymer nanocomposite is fabricated using a blend of high density/ultrahigh molecular weight polyethylene with magnetite nanoparticle (MNP) fillers. The resulting magnetite–polyethylene nanocomposite (MPE-NC) is mechanically robust and can be externally actuated with an alternating magnetic field to generate localized heating that is effective in eradicating bacterial biofilms. The MNPs are functionalized with silane-based coupling agents and crosslinked onto the polyethylene backbone via a reactive extrusion approach, which results in a twofold enhancement in mechanical properties of the polymer matrix. Furthermore, the magnetic hyperthermia performance of the MPE-NC is improved eightfold by replacing undoped magnetite nanospheres with zinc-doped magnetite nanocube fillers, and the magnetic hyperthermia treatment approach is shown to be 12 times more effective in destroying bacterial biofilms compared to a direct heat-treatment method. During hyperthermia treatment, the mechanical integrity of the MPE-NC is preserved, thereby validating the potential of the MPE-NC as a new filter material with high efficiency in biofilm removal and extended durability.

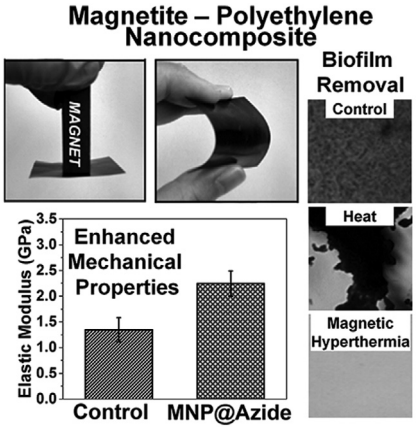

Dr. S. F. Situ, C. Chen, E. C. Abenojar, Prof. A. C. S. Samia
Department of Chemistry
Case Western Reserve University
10900 Euclid Avenue, Cleveland, OH 44106, USA
E-mail: anna.samia@case.edu
J. Cao, Prof. J. M. Maia
Department of Macromolecular Science and Engineering
Case Western Reserve University
10900 Euclid Avenue, Cleveland, OH 44106, USA
E-mail: joao.maia@case.edu

1. Introduction

Water contamination remains a major global public health concern causing over 2 million deaths annually.[1,2] The water filtration unit is an elaborate system that has been employed heavily in recycling wastewater for both industrial and domestic usage.[2,3] Polyethylene (PE), is commonly used to fabricate various parts of the filtration unit in durable water filtration systems, such as the filter

Macromol. Mater. Eng. **2016**, DOI: 10.1002/mame.201600249

membrane, membrane housing, reservoir tanks, and pipe tubings, due to its robust mechanical properties and chemical stability.[4–8] One of the major challenges in preserving the mechanical integrity and extending the lifetime of PE-based filter units is biofouling, which causes over 45% of premature filtration system failures.[1,9–11] Biofilm buildup on the filter surface can negatively impact the recycled water quality, causing potential bacterial contamination and significantly reducing the flux of water flow.[12–14] In addition to decreasing the filtration system performance, overgrowth of biofilms can also lead to the biodegradation of the PE components, with some types of bacterial cells able to utilize the carbon from the polymer as an energy source, thus leading to the polymer's early deterioration.[15] Due to the tight network of the biofilm structure, commonly used antibiotics cannot easily penetrate through the biofilm to effectively eradicate the microbial colonies.[16] While adding a disinfection cycle to the wastewater feed prior to passing through the filter system can remove most of the bacterial cells, a small amount of viable microbes remaining in the feed can self-replicate and grow exponentially to form hard-to-treat biofilms.[16] Furthermore, due to the hydrophobic nature of PE, bacterial cells have a strong tendency to adhere to the polymer surface, thereby increasing the likelihood of biofilm formation.[17] Therefore, significant efforts have been devoted toward finding effective methods to eradicate biofilm networks found in water filtration systems.[18] Conventional treatment methods using concentrated alkali, acidic, or chlorinated solutions can leave behind chemical residues and induce oxidation of the PE material, while hydraulic cleaning methods with high pressure water or air can cause physical damage to the filtration system.[19–21] Over the past decades, UV-ozone treatment has been adapted as a standard cleaning approach for water filters to deactivate biofilm growth.[22] However, repeat exposures to UV-ozone can induce polyolefin oxidation leading to premature fragmentation of the PE backbone, which shortens the lifetime of the filtration system.[23] Recently, magnetic hyperthermia has been investigated for its potential in antibacterial applications and has been demonstrated as an effective method to thermally inactivate bacterial planktonic cells and biofilms.[24–26] Such thermal inactivation mechanism does not rely on the therapeutic efficacy of antibiotics, therefore making magnetic hyperthermia-based disinfection methods especially attractive for treating bacterial strains with antibiotic resistance.[24–26] By incorporating magnetic nanoparticles into the PE matrix, we are able to exploit the unique properties of the magnetic nanoparticles and its capability to generate heat upon exposure to an alternating current (AC) magnetic field. In this study, we report on the fabrication of a novel magnetically responsive smart polymer nanocomposite with high efficiency toward bacterial biofilm removal. Using a blend of high density and ultrahigh molecular weight polyethylene with magnetite nanoparticle (MNP) fillers, we were able to fabricate a mechanically robust magnetite–polyethylene nanocomposite (MPE-NC) that can be externally actuated with an AC magnetic field to generate localized heating, which is effective in eradicating bacterial biofilms. The MNPs were functionalized with silane-based coupling agents to facilitate the crosslinking of the MNPs onto the polyethylene backbone through a reactive extrusion processing approach.

The physical and chemical properties of previously fabricated magnetic nanocomposites have been shown to be directly linked to the amount of magnetic nanoparticle fillers incorporated in the polymer matrix.[27–30] A higher loading of magnetic nanoparticle fillers results in enhanced magnetic responsiveness; however, the mechanical performance of the polymer matrix is negatively impacted upon increase in nanoparticle loading.[28] While the addition of low amounts of nanoparticle fillers can enhance the mechanical properties by improving stress transfer from the soft polymer matrix to the stiffer nanoparticle fillers, a higher loading of nanoparticle fillers can significantly weaken the mechanical properties due to reduced interactions between the polymer strands.[30] Therefore, ensuring good interfacial interactions between the MNPs and PE matrix is an important factor to consider in order to preserve the mechanical properties of the polymer matrix at high filler loadings.

To date, numerous studies have introduced additional reagents as compatibilizers or coupling agents during the melt-blending processing of polymer nanocomposites in order to increase the interfacial interactions between the nanosized fillers and the polymer matrix.[31–38] Among these approaches, silane coupling agents have been demonstrated to effectively improve the interfacial interactions between the polymer matrix and various types of nanosized fillers such as SiO_2, Al_2O_3, $CaCO_3$, and carbon nanotubes.[37–47] In particular, vinylsilane coupling agents have been extensively used to facilitate crosslinking in thermoplastic nanocomposites with the addition of a peroxide initiator.[48] During the reactive extrusion process, the peroxide initiator first decomposes at elevated temperatures to form oxyradicals. The oxyradical has the ability to abstract hydrogen from the thermoplastic backbone, which in turn can propagate a radical chain reaction leading to the crosslinking of the fillers to the thermoplastic matrix.[40,47–52] On the other hand, azidosilane coupling agents have also attracted significant interests in the fabrication of polymer nanocomposites, due to its ability to form reactive nitrenes at elevated temperatures (>110 °C) without the need for a peroxide initiator.[40,53] Eliminating the need for a peroxide initiator during the crosslinking reaction can minimize oxidative damage to the thermoplastic matrix,

which can help prevent the mechanical weakening of the fabricated nanocomposite.[39,51] In this study, the effect of vinyl- and azido-silane coupling agents on the mechanical and rheological properties of the MPE-NCs was investigated. The as-synthesized MNPs are capped with oleic acid ligand, which can facilitate van der Waals interaction with the PE strands. To facilitate covalent linkage between the MNP fillers and the PE backbone, the MNP were first functionalized with 7-octenyltriethoxysilane or 6-azidosulfonylhexyltriethoxysilane containing vinyl- and azido-terminal groups, respectively. In the case of the MNPs functionalized with the vinylsilane coupling agent, dicumyl peroxide (DCUP) was used as the peroxide initiator to induce the radical formation on the vinyl terminal group.[54,55] As for the MNP functionalized with the azidosilane coupling agent, the reactive nitrene can be activated thermally without addition of a peroxide initiator.[53,56] The fabricated MPE-NCs were characterized by evaluating their mechanical, rheological, thermal, and magnetic properties. Furthermore, the MPE-NCs' ability to eradicate biofilm networks were investigated and their mechanical properties after exposure to AC field excitation and UV-ozone treatments were compared.

2. Results and Discussion

2.1. Synthesis and Functionalization of the Magnetite (Fe_3O_4) Nanoparticles

The MNPs with an average diameter of 15 nm were synthesized using a modified thermal decomposition method.[57–61] The as-synthesized MNPs are capped with oleic acid ligand and display monodisperse size and spherical shape as evident from the obtained transmission electron microscope (TEM) images (Figure 1a). In addition to the oleic acid capped MNPs, the MNPs functionalized with the two different silane coupling agents, 7-octenyltriethoxysilane and 6-azidosulfonylhexyltriethoxysilane, were prepared by using a modified ligand exchange approach (see Experimental Section). The TEM images of the vinylsilane and azidosilane functionalized MNPs indicate that the nanoparticle morphology and size have not been altered during the surface modification steps (Figure 1a). The crystalline phases of the as-synthesized and silane-functionalized MNPs were evaluated using powder X-ray diffractometry (PXRD) and was demonstrated to be that of the magnetite (Fe_3O_4) phase (Figure 1b), which is the iron oxide crystal phase with the highest saturation magnetization (M_s) value of ≈92 emu g^{-1} in the bulk material.[62] The successful silane-functionalization of the MNPs was verified from the obtained IR spectra (Figure 1c). In the oleic acid capped MNPs (MNP@OA), two strong peaks appear at 1734 and 2926 cm^{-1} corresponding to the vibrational stretching of

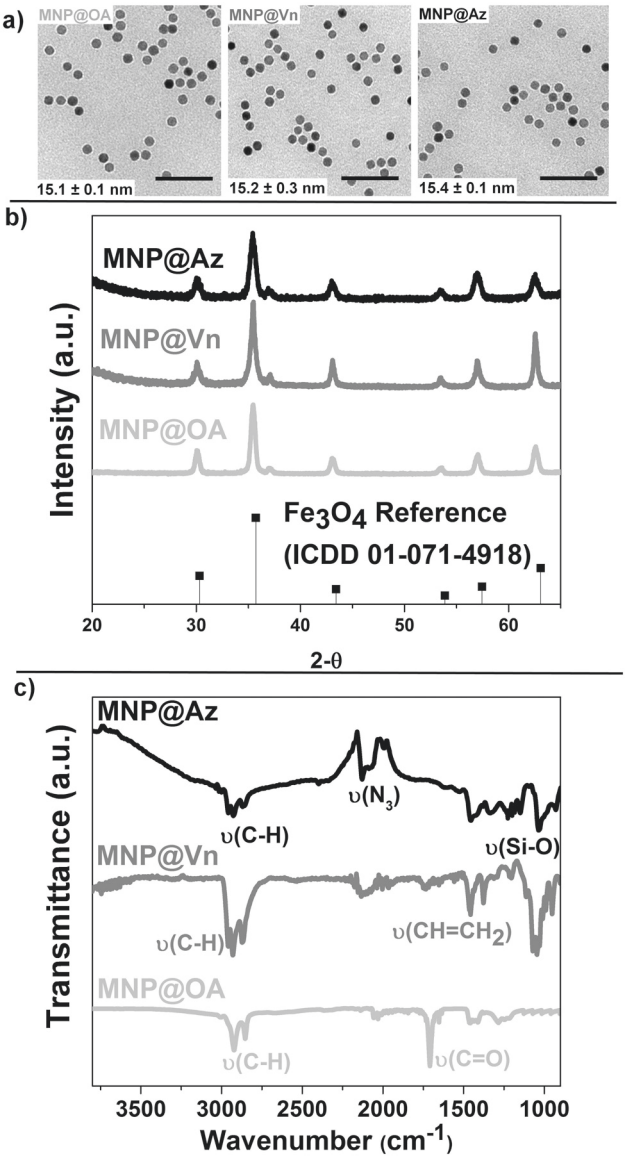

Figure 1. a) TEM images of the oleic acid capped magnetite nanoparticles (MNP@OA), vinyl-functionalized magnetite nanoparticles (MNP@Vn), and azide-functionalized magnetite nanoparticles (MNP@Az). Scale bars represent 100 nm. The corresponding b) PXRD and c) FTIR spectra of the magnetite nanoparticles.

C=O and C—H in oleic acid, respectively. After surface modification following the ligand exchange process, the characteristic peak for the Si—O vibrational stretch becomes apparent in the vinylsilane-(MNP@Vn) and azidosilane-(MNP@Az) functionalized MNPs, indicating the effective substitution of the oleic acid ligand with the silane coupling agents. Moreover, the presence of characteristic peaks for the vibrational stretching for vinyl ($-CH=CH_2$) at 1492 cm^{-1} and azide ($-N_3$) at 2095 cm^{-1} further confirm the effective surface modification of the MNPs. The ligand coverage in the silane-functionalized MNPs was estimated from results obtained from thermogravimetric

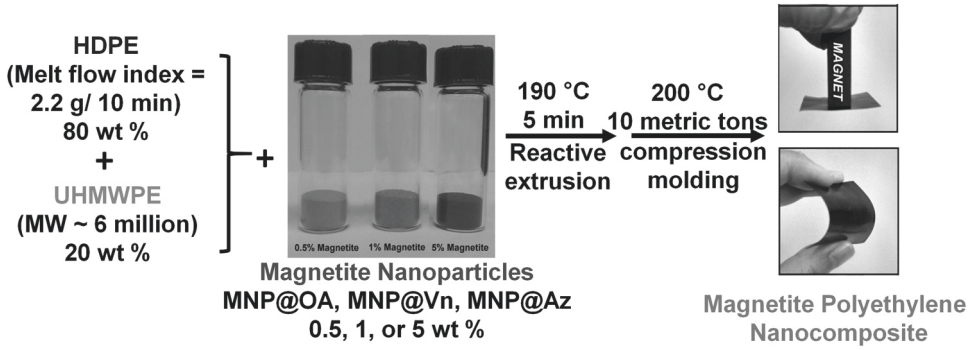

Scheme 1. Overview of the reactive extrusion and compression molding processes used in the fabrication of the magnetite–polyethylene nanocomposites.

analysis (TGA) (Figure S1, Supporting Information). The amount of vinylsilane and azidosilane found in the modified MNPs were estimated to be 13.8 and 9.6 wt%, respectively. In the MNP@Vn sample, the number of vinylsilane molecules per individual MNP was found to be around 4530, which translates to an average surface area coverage of 6.41 vinylsilane molecules per nm^2 of the MNP. On the other hand, the number of azidosilane molecules was estimated to be 2232 per MNP and a surface area coverage of ≈3.16 molecules per nm^2 was calculated for the MNP@Az sample (Table S1, Supporting Information). These results indicate that significant amounts of silane coupling agents were successfully grafted onto the surface of the MNPs.

2.2. Reactive Extrusion of the Magnetite–Polyethylene Nanocomposites

High-density polyethylene (HDPE, Melt Flow Index = 2.2 g per 10 min, Sigma-Aldrich, USA) was chosen as the polymer matrix in our study due to its excellent processability, low cost, and good chemical properties. In order to improve the mechanical properties of the final composite, while keeping it melt processable by extrusion, 20% w/w of ultrahigh molecular weight PE (M_W ≈ 3–6 million, Sigma-Aldrich, USA) was melt blended into the HDPE matrix (Scheme 1). To facilitate the crosslinking of the silane-functionalized MNPs onto the PE backbone, we adopted a reactive extrusion approach. The thermal stability of oleic acid, vinylsilane, and azidosilane were evaluated using an attenuated total reflectance-Fourier transform infrared (ATR-FTIR) spectrometer setup. The oleic acid ligand and the vinylsilane coupling agent were stable up to 230 °C (Figure S2a,b, Supporting Information). On the other hand, the intensity of the azide vibrational stretch at 2095 cm^{-1} decreased dramatically as the temperature increased, and the signal disappeared completely after exposure to temperatures higher than 190 °C (Figure S2c, Supporting Information). The observed instability of the azide functional group at higher temperatures is consistent with previously reported studies.[36,47] Therefore, for the reactive extrusion processing step, the extrusion temperature was selected to be 190 °C to efficiently integrate the MNP fillers and the PE while preventing the degradation of the azidosilane coupling agent. Subsequently, the nanocomposite films used in the mechanical testing and biofilm studies were prepared through a compression molding processing approach using a Carver Benchtop Press that utilized a heating stage set at 200 °C and under 10 metric tons of applied pressure.

To examine the effects of the reactive extrusion and compression molding processing on the morphology of the MNP fillers, micron-sized debris were obtained from the MPE-NCs and imaged under TEM. It is evident that the morphology of the MNP fillers was not altered during NC processing (Figure S3a,b, Supporting Information). Furthermore, the MNP fillers were found to be more evenly distributed throughout the compression molded MPE-NC processed through reactive extrusion (Figure S3a, Supporting Information) compared to the NC fabricated without adopting a reactive extrusion approach (Figure S3b, Supporting Information). Moreover, the field-dependent magnetic property of the MNPs was not affected after the reactive extrusion and compression molding processing steps (Figure S3c, Supporting Information).

2.3. Effects of Reactive Extrusion on Polyethylene Oxidation

During the reactive extrusion of MNP@Vn and PE, 0.05% DCUP was introduced to generate reactive radicals on the vinylsilane moieties in order to form the covalent linkage with the PE backbone. Although DCUP has been widely used as a peroxide initiator in similar crosslinking reactions, DCUP can also induce oxidation in the PE backbone, which can lead to weakening of the mechanical properties of the polymer.[42] The possible oxidation in nanocomposite films fabricated with MNP@OA, MNP@Az, and MNP@Vn was evaluated using an ATR-FTIR system. The IR spectrum of the nanocomposite fabricated with MNP@Vn fillers with DCUP initiator revealed the highest observed intensity that is characteristic of the C=O vibrational

stretch, indicating the oxidative conversion from polyolefin to carbonyl terminating structures (Figure S4, Supporting Information), which can compromise the mechanical properties of the PE matrix.[63–66] On the other hand, oxidation of the PE matrix was not evident in the IR spectra obtained from the nanocomposite films fabricated with MNP@OA and MNP@Az fillers, thereby confirming that MNP@Az is an ideal filler candidate for increasing the interfacial interaction between the MNP fillers and the PE matrix with minimum oxidation effects on the polymer backbone.

2.4. Mechanical Properties of the Magnetite–Polyethylene Nanocomposites

The mechanical properties of the fabricated MPE-NCs were evaluated by measuring the elastic modulus and hardness using an Agilent Keysight Nano-Indenter system. As seen in Figure 2, no significant change in elastic modulus and hardness was observed in the MPE-NCs fabricated with MNP@OA fillers (labeled as MNP@OA-PE in Figure 2). This result can be attributed to oleic acid's limited chemical interaction with the PE backbone. The van der Waals interaction between MNP@OA and the PE backbone was not sufficient to improve the mechanical properties of the polymer blend. Similarly, no significant enhancement in mechanical property was observed for the nanocomposites containing MNP@Vn fillers (labeled as MNP@Vn-PE in Figure 2). In utilizing the vinylsilane coupling agent, the presence of the peroxide initiator has been previously shown to induce PE oxidation (Figure S4, Supporting Information), which have been demonstrated to cause mechanical embrittlement of PE-based materials.[66] On the other hand, a twofold increase in elastic modulus and a threefold enhancement in hardness was observed for the MPE-NCs containing MNP@Az fillers (labelled as MNP@Az-PE in Figure 2). This can be explained by the capability of the MNP@Az fillers to be thermally activated and crosslinked to the PE matrix without causing significant oxidative damage to the PE backbone.

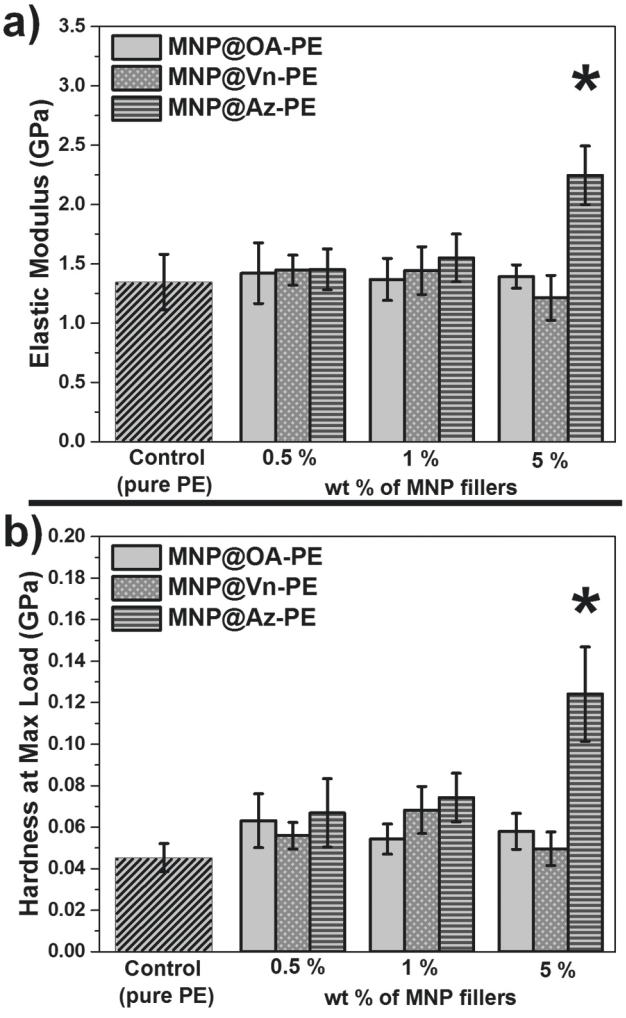

Figure 2. The a) elastic modulus and b) hardness at maximum loading values of the magnetite–polyethylene nanocomposites fabricated with oleic acid capped magnetite nanoparticles (MNP@OA-PE), vinyl-functionalized magnetite nanoparticles (MNP@Vn-PE), and azide-functionalized magnetite nanoparticles (MNP@Az-PE). The asterisk indicates that the results were determined to be statistically significant from the control sample with *p*-value less than 0.05 using Student's *t*-test.

2.5. Rheological Properties of the Magnetite–Polyethylene Nanocomposites

The storage (G′) and loss (G″) moduli of the fabricated MPE-NCs were measured at 190 °C. To evaluate the viscoelastic properties of the MPE-NCs, the tan δ (G″/G′) was calculated at 1 rad s^{-1} and the change in tan δ as a function of MNP filler loading is presented in Figure 3a. The tan δ values for all fabricated MPE-NC blends increase with increasing loading of MNP fillers with a value above 1 observed for the nanocomposite with 5% MNP@OA filler loading, signifying liquid-like behavior. On the other hand, the tan δ value of the MPE-NC fabricated with 5% MNP@Vn fillers was estimated to be around 1, a result of equal G″ and G′ values, representing a phase transition from liquid-like to solid-like behavior. At 5% MNP@Az filler loading, a tan δ value below 1 was observed, indicating a solid-like behavior for the fabricated MPE-NC at high loading of MNP@Az fillers (Figure 3a and Figure S5, Supporting Information). This rheological behavior supports the enhanced mechanical properties observed for the MPE-NC fabricated with 5% MNP@Az.

2.6. Thermal Properties of the Magnetite–Polyethylene Nanocomposites

In addition to studying the rheological properties, the thermal properties of the MPE-NCs were evaluated using

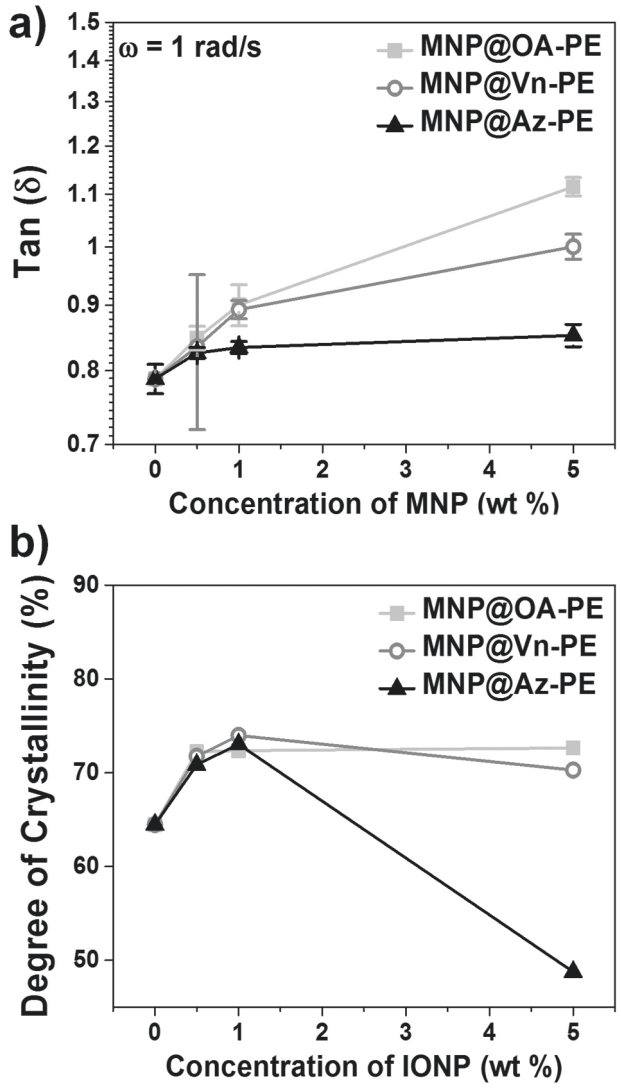

Figure 3. a) Rheological properties of the magnetite–polyethylene nanocomposites fabricated with 0, 0.5, 1, and 5 wt% of oleic acid capped magnetite nanoparticles (MNP@OA-PE), vinyl-functionalized magnetite nanoparticles (MNP@Vn-PE), and azide-functionalized magnetite nanoparticles (MNP@Az-PE) as fillers. The tan(δ) values were calculated from the storage and loss modulus at an angular frequency of 1 rad s^{-1}. b) The corresponding degree of crystallinity, estimated from differential scanning calorimetry measurements.

differential scanning calorimetry (DSC). Overall, the inclusion of MNP fillers caused a slight increase in the degree of crystallinity. However, at the highest loading of MNP@Az fillers (5%), a drastic 33% decrease in the degree of crystallinity was observed for the fabricated MPE-NC (Figure 3b and Figure S6, Supporting Information). This result can be attributed to the increase in PE crosslinking, leading to less ordered polymer network structures. The enhanced crosslinking in the MNP@Az-PE nanocomposite also explains the observed improvements in mechanical properties, even though the overall crystallinity is lower (Figure 2).

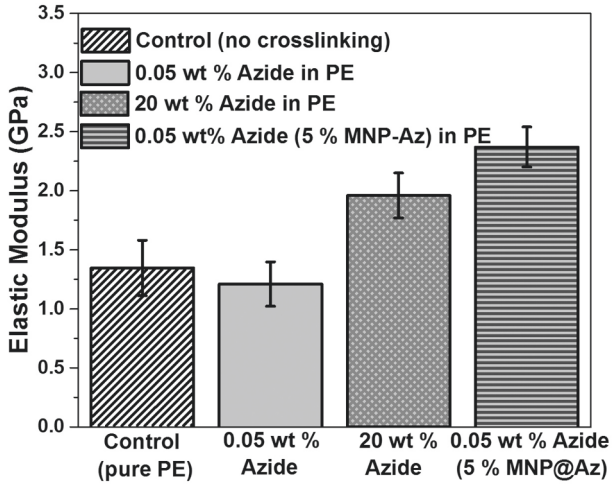

Figure 4. The elastic modulus of the azide crosslinked polyethylene nanocomposites fabricated with and without magnetite nanoparticles.

2.7. Investigation of the Azide Coupling

As previously reported, azidosilane coupling agents can bind to thermoplastic polymers through a nitrene-mediated C—H bond amination process, which can be facilitated by thermal activation and/or transition metal catalysis.[67,68] In this case, the high level of Fe ions available from the MNPs can serve as the catalyst during the azide coupling reaction between the MNP@Az fillers and the PE backbone. To explore the coupling chemistry route for the MPE-NCs fabricated using the MNP@Az fillers, we first investigated the effect of azidosilane in the crosslinking of the PE matrix in the absence of the MNP fillers. In the absence of MNP fillers, no change was observed in elastic modulus when 0.05 wt% of azidosilane coupling agent was added (the equivalent amount of azidosilane added in the MPE-NC with 5% MNP@Az fillers) (Figure 4). An increase in elastic modulus was only observed in the extruded PE after the addition of a high concentration of azidosilane coupling agent at 20 wt%. On the other hand, upon adding 5% of the MNP@Az fillers, the elastic modulus was enhanced twofold compared to the PE matrix fabricated with the same amount of azidosilane coupling agent (0.05%) in the absence of MNP (Figure 4). The mechanical property enhancement observed for the MNP@Az-PE due to higher crosslinking by the azidosilane coupling agent in the presence of MNPs is an indication of the role that Fe can play in catalyzing the formation of the reactive nitrene groups.

2.8. Magnetic Hyperthermia Performance of the MPE-NCs

For the succeeding studies, we have adapted the use of the MNP@Az fillers in the fabrication of the MPE-NCs

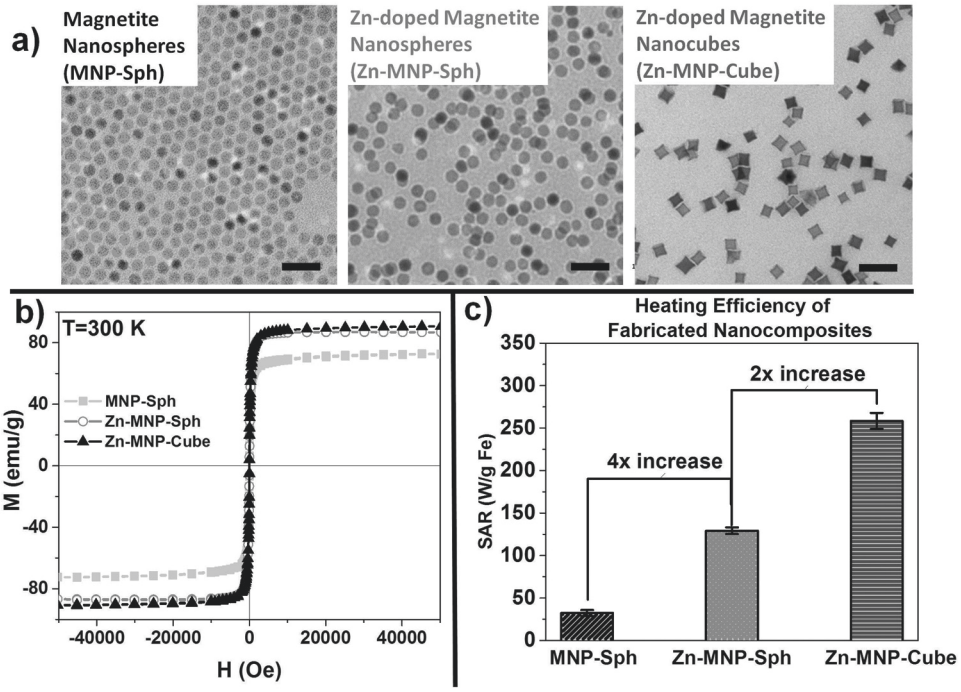

Figure 5. a) The TEM images of magnetite (Fe_3O_4) nanospheres, Zn-doped magnetite ($Zn_{0.4}Fe_{2.6}O_4$) nanospheres, and Zn-doped magnetite ($Zn_{0.4}Fe_{2.6}O_4$) nanocubes, respectively. Scale bars represent 50 nm. b) The corresponding field-dependent magnetization curves of the magnetite nanoparticles measured at 300 K. c) The calculated SARs estimated from the magnetic hyperthermia measurements of the fabricated magnetite–polyethylene nanocomposites prepared using the different types of magnetite nanoparticle fillers. All hyperthermia measurements were performed at a concentration of 1 mg Fe mL^{-1}, $H = 60$ kA m^{-1}, and $f = 380$ kHz, and the reported SAR values were averaged from three trials.

since it leads to the best mechanical performance at the highest filler loading at 5%. The magnetic hyperthermia performance of the fabricated MPE-NCs was evaluated by measuring the change in temperature under AC magnetic field excitation. The heating efficiency was assessed by estimating the specific absorption rate (SAR) based on the obtained temperature curves during AC field exposure. Embedding the MNPs in the polyethylene matrix prevented nanoparticle rotation, which in turn reduced the heating efficiency (lower SAR value) due to suppressed Brownian relaxation (Figure S7, Supporting Information). Since optimizing the heat generation efficiency of the MPE-NC will be essential for its ability to effectively eradicate bacterial biofilms, it is paramount to tune the magnetic properties of the MNP fillers in order to enhance the magnetic hyperthermia performance of the nanocomposites. To improve the magnetic hyperthermia performance of the MPE-NCs, the magnetic properties of the MNP fillers were first tuned by selectively replacing the Fe^{2+} ions in the tetrahedral sites within the spinel ferrite lattice with diamagnetic Zn^{2+} ions, thus, resulting in an increase in the net magnetic moment of the overall magnetite system.[69,70] Previous studies have demonstrated that the maximum M_s value is achieved by tuning the atomic ratio of the zinc to iron ions to 0.4:2.6 (13% zinc dopant).[70] The zinc-doped spherical magnetite ($Zn_{0.4}Fe_{2.6}O_4$) nanoparticles with an average diameter of 15 nm were synthesized by varying the metal precursor (Figure 5a). The resulting spherical MNP fillers containing 13% zinc-dopant led to a 21% enhancement in the M_s value obtained from field-dependent magnetic measurements (Figure 5b). The MPE-NC fabricated with zinc-doped magnetite nanospheres exhibited a fourfold increase in SAR value, achieving a maximum temperature of 64 °C (Figure 5c and Figure S8, Supporting Information). To further enhance the magnetic performance of the MPE-NCs, zinc-doped magnetite nanocubes with volumes that are equivalent to their spherical counterparts were used in the fabrication of the nanocomposites and the M_s value of the resulting MPE-NC was estimated to be 92 emu g^{-1}, a 28% increase in M_s value compared to MPE-NC fabricated with undoped magnetite nanospheres (Figure 5a,b). The MPE-NC fabricated with zinc-doped magnetite nanocubes demonstrated an additional twofold increase in SAR (an overall eightfold increase in SAR compared to undoped magnetite nanospheres) and a maximum temperature rise of 93 °C was reached (Figure 5c and Figure S8, Supporting Information), which is sufficient to thermally deactivate the most common bacterial strains (i.e., *Pseudomonas* at 85 °C for 1 min, *Salmonella* at 54 °C for 5 min, *Listeria* 80 °C for 12 min and *Escherichia coli* at 50–70 °C for 15 min).[71–74]

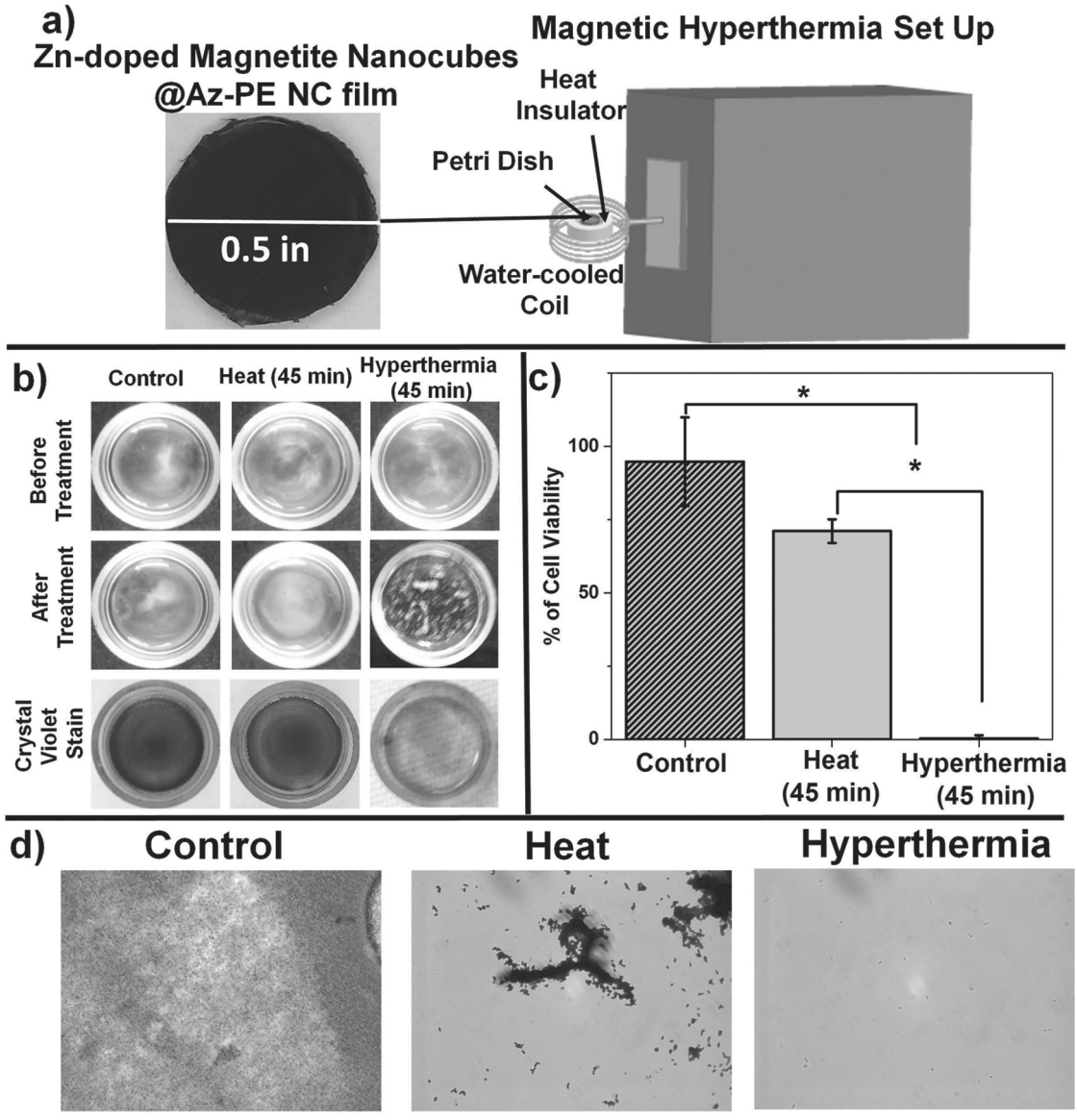

Figure 6. a) The schematic illustration of magnetic hyperthermia treatment setup used in the biofilm eradication study. b) Photographs of biofilm cultures subjected to different treatment methods; no treatment, direct heating for 45 min at 90 °C, and magnetic hyperthermia treatment with magnetite–polyethylene nanocomposite for 45 min. The asterisk indicates that the results were determined to be statistically significant from each other with *p*-value less than 0.05 using Student's *t*-test. The biofilm cultures post-treatment were stained with crystal violet dye. c) Percentage of bacteria cell viability of biofilm post-treatments. d) Optical microscopy images of the crystal violet stained biofilms post-treatments.

2.9. Application of the MPE-NCs in Biofilm Eradication

To assess the effectiveness of the magnetic hyperthermia treatment approach in destroying bacterial biofilms, a bench top magnetic hyperthermia setup with a water-cooled coil that operates at 380 kHz with field strength of 60 kA m^{-1} was utilized. A circular MPE-NC film with 0.5 inch diameter was placed on top of the biofilm grown within a custom made glass dish that was placed inside an insulating holder prior to magnetic hyperthermia treatment (Figure 6a). The MPE-NC fabricated with azide functionalized zinc-doped magnetite nanocubes was chosen for this test due to its ability to reach above 90 °C within 45 min of AC field excitation, and all treatment conditions described here were repeated three times (Figure S8, Supporting Information). As seen in Figure 6b, subjecting the biofilm culture to magnetic hyperthermia treatment for 45 min through exposure to the MPE-NC leads to the optimal removal of the biofilm, as evident from the significantly reduced crystal violet staining of

Macromolecular Journals
Macromol. Mater. Eng. **2016**, DOI: 10.1002/mame.201600249

the remaining bacterial cells after hyperthermia exposure. Meanwhile, the control (no treatment) biofilm samples and the biofilm samples exposed to direct heat-treatment (90 °C in convection oven) retain full coverage of biofilm network on the glass dish surface, indicating that direct heat application was not effective in biofilm removal. Furthermore, the percentage of cell viability was determined by measuring the absorbance of the crystal violet dye that was used to stain the remaining bacterial cells, demonstrating a 71.1% and 0.5% of cell viability after direct heating and magnetic hyperthermia treatments, respectively (Figure 6c). Although both the application of direct heating and magnetic hyperthermia resulted in similar global temperatures for the biofilm culture environment, the higher reduction in cell viability upon exposure to magnetic hyperthermia heating can be explained by an enhanced localized heating generated in the MPE-NC, which can lead to a more effective destruction of the biofilm network. To verify the reduction in cell viability caused by magnetic hyperthermia heating from the MPE-NC, additional experiments were conducted in two different conditions to examine the individual effects of AC magnetic field exposure and contact of the MPE-NC on the biofilm. When the biofilm culture was exposed to the AC magnetic field in the absence of the MPE-NC, no significant heating was observed and the biofilm network remained attached to the glass dish surface, which translated to a 100% cell viability compared to the control biofilm culture receiving no treatment. (Figure S9, Supporting Information). Similarly, 100% cell viability was also observed when the biofilm culture was incubated with the MPE-NC film without applying an external AC magnetic field. These results demonstrate that the combined effect of the MPE-NC film and AC magnetic field exposure is crucial in the heat generation process in order to effectively eradicate the biofilm network. Moreover, the crystal violet stained biofilms were imaged using a Leica DM6000 upright bright-field microscope. As seen in Figure 6d, the biofilm network of the control sample appears to be highly populated with bacterial cells that are connected in a tight network. After exposure to a direct heat treatment method, the biofilm network appears to be broken, but large debris with high number of bacterial cells was still observed. On the other hand, the biofilm exposed to magnetic hyperthermia treatment show significantly fewer and smaller biofilm debris and bacterial cells are lightly stained by the crystal violet dye. These images of biofilm treated with different methods demonstrated that the localized heat generation from the MPE-NC is more effective in biofilm eradication than the directing heating approach.

2.10. Effect of Magnetic Hyperthermia Treatment on the Mechanical Properties of the MPE-NCs

To examine the effect of AC magnetic field exposure on the properties of the MPE-NCs, the mechanical properties of the nanocomposites subjected to magnetic hyperthermia treatment were investigated and compared to direct heating and UV-ozone treatments. Moreover, the treatment effects on the chemical oxidation of the PE matrix were evaluated using IR spectroscopy. After three repeat cycles of 30 min treatment, a clear C=O vibrational stretch was evident in the MPE-NC treated with UV-ozone, while no visible peak from PE oxidation was observed in the MPE-NCs treated with magnetic hyperthermia or direct heating (Figure 7a,b). Such increase in PE oxidation caused by UV-ozone treatment also manifested in the mechanical properties of the MPE-NCs, with a 50% reduction in the elastic modulus observed in MPE-NC post UV-ozone treatment (Figure 7c). On the other hand, treating the MPE-NCs

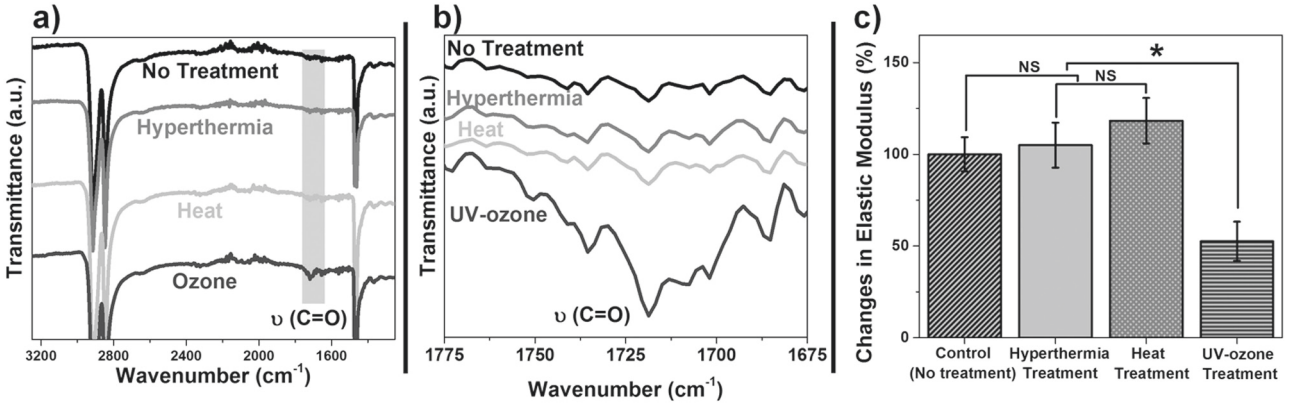

Figure 7. a) The FTIR spectra of the magnetite–polyethylene nanocomposites after exposure to ambient environment as a control, and repeated cycles of magnetic hyperthermia, direct heating, and UV-ozone treatments. b) The zoom-in FTIR spectra highlighting the C=O vibrational stretch peak at 1720 cm^{-1}. c) Percentage changes in elastic modulus of the treated magnetite–polyethylene nanocomposites compared to the control untreated sample. The asterisk indicates that the results were determined to be statistically significant and NS represents results that were not statistically significant from each other with *p*-value less than 0.05 using Student's *t*-test.

with magnetic hyperthermia or direct heating did not cause significant reduction in the mechanical properties of MPE-NCs post-treatment, which demonstrates the shelf-life of filter materials made from MPE-NCs can be potentially extended if magnetic hyperthermia is adapted to remove biofilm network from the filter system.

3. Conclusions

In summary, we were able to fabricate mechanically robust and magnetically responsive polymer nanocomposites using silane-functionalized MNP fillers through a reactive extrusion approach. The azido-terminated MNPs provided the optimum enhancement in mechanical properties of the polymer matrix through an iron-catalyzed nitrene crosslinking chemical route. Moreover, optimal magnetic hyperthermia performance was observed upon tuning the composition and shape of the MNP fillers, and an eightfold increase in heating efficiency was observed for the MPE-NC fabricated using zinc-doped magnetite nanocubes. A comparison of the magnetic hyperthermia biofilm eradication approach with direct heating and conventional UV-ozone treatment methods, demonstrated the effectiveness of the magnetic hypethermia method in destroying biofilm growth, while preserving the mechanical integrity of the polyethylene matrix. Thus, this study demonstrates the potential of magnetite–polyethylene nanocomposites in the development of functional water filter materials with excellent mechanical properties.

4. Experimental Section

4.1. MNP Synthesis and Surface Functionalization

MNPs were synthesized using a modified thermal decomposition method.[57–61] The size, shape, and chemical composition of the nanoparticles can be controlled by varying the type and concentration of metal precursors, capping ligand, and reaction heating rate. The as-synthesized MNPs are capped with oleic acid and were subsequently modified with two different silane coupling agents: 7-octenyltrimethoxysilane and 6-azidosulfonylhexyltriethoxysilane, both were purchased from Gelest Inc. and used as received. In order to attach the silane coupling agents onto the surface of the MNPs, the silane coupling agents (2 mL) were first hydrolyzed in DI water (2 mL) at 70 °C for 2 h. After hydrolysis, the oleic acid capped MNPs (2 g) in 40 mL of toluene, NH_4OH in 1-butanol (40 mL), and trimethylamine (15 mL) were added to the reaction mixture and the mixture was stirred at 70 °C for an additional 6 h. The resulting functionalized MNPs were separated by centrifugation and dispersed in dimethylformamide. The ligand coverage was estimated based on the results obtained from TGA using a method previously reported by Liu et al.[75]

4.2. MNP-PE Nanocomposite Fabrication

The reactive extrusion process was completed using a HAAKE MiniLab II Micro Compounder with co-rotating conical twin-screws. The MNP fillers with different silane terminal groups were integrated at 0.5, 1, and 5 wt% loading into a polyethylene blend containing 80% HDPE and 20% UHMWPE. All samples were extruded for 5 min at 190 °C at a 60 rpm rotational rate. The composite strips obtained from the reactive extrusion were then cut into small pellets and fabricated into circular films by a compression molding method. The composite pellets were melted at 200 °C inside a custom-made aluminum mold lined with PTFE linings. The pressure was then gradually increased to 10 metric tons and held at that pressure for 5 min. This compression step was repeated twice to achieve an even molded surface. The final composite film has a thickness of about 0.015 in.

4.3. Mechanical Testing through Nanoindentation

The elastic modulus and hardness of the nanocomposite films were measured by using the G 200 Nano Indenter from Keysight using a Berkovich diamond indenter with loading/unloading rate of 2 mN s^{-1} and Poisson ratio of 0.46. The nanocomposite films were cut into 3 mm by 3 mm strips and 16 indents were performed for each sample.

4.4. Rheological Property Evaluation

The rheological properties of the fabricated nanocomposites were evaluated at 190 °C using a strain controlled Rheometrics RMS 800 rheometer (Rheometrics, USA) with a 25 mm parallel plate fixture. The angular frequency was sweep from 100% to 0.1% to obtain the storage and loss modulus of the nanocomposites. The samples were fabricated into a circular film with 25 mm diameter and 1 mm thickness using compression molding on a bench top Carver Press (CH4386).

4.5. Evaluation of the Degree of Crystallinity

The degree of crystallinity of the fabricated nanocomposites was investigated by measuring the enthalpy of fusion of the nanocomposites relative to a 100% polyethylene crystal standard (293 J g^{-1}). The enthalpy of fusion of our samples was measured using a Q2000 TA DSC.

4.6. Biofilm Formation

The biofilm culture was prepared using a method adapted from the previous study of Duncan et al.[76] The *E. coli* cells were first cultured in lysogeny broth (LB) medium at 37 °C. After the culture reached the stationary phase, the cells were collected and washed with 0.85% NaCl solution for a total of three times. The resulting bacterial cell pellet was resuspended in a modified LB broth containing 0.1% glucose, 1×10^{-3} M $MgSO_4$, 0.15 M ammonium sulfate, 34×10^{-3} M citrate, and the LB medium was buffered to pH 7 to increase the adhesion between the bacterial cells

Macromol. Mater. Eng. **2016**, DOI: 10.1002/mame.201600249

and glass dish surface to promote biofilm formation. The suspended bacteria seeding solution was adjusted to a concentration of 0.1 at $O.D._{600}$. An aliquot with 500 μL of the seeding solution was added to each custom glass petri dish (2.5 cm O.D.) and an additional 1 mL of modified LB medium was added before covering the glass dish and incubating the culture at room temperature for 72 h. The LB media in the culture dish was exchanged with 1.5 mL of fresh modified LB medium on the second day of incubation.

4.7. Magnetic Hyperthermia Treatment of Biofilm

The matured biofilm was gently washed with DI water three times to removed detached bacteria cells. After washing, a circular magnetic polyethylene composite film (1 cm diameter) was place on top of biofilm and 1 mL of DI water was added to submerge the film. The glass dish was then placed in the middle of the water-cooled coil exposed to an AC magnetic field excitation at a fixed frequency (f) of 380 kHz and magnetic field amplitude (H) of 60 kA m^{-1} for magnetic hyperthermia treatment for 45 min. After the magnetic polymer composite film was removed from the glass dish, the biofilm was gently rinsed with DI water three times to remove detached bacteria cells. All treatment conditions were repeated three times.

4.8. Crystal Violet Staining and Determination of Cell Viability

After exposure to the different treatment methods, the biofilms were incubated in 500 μL of 0.1% crystal violet solution for 30 min. The stained biofilms were then washed three times with DI water and dried before taking photograph images. For the quantitative determination of the cell viability, 500 μL of acetic acid in water was added to each dish to solubilize the crystal violet within the stained attached bacterial cells. The solution was then diluted 10 times prior to measuring the absorbance at 550 nm using a FLUOstar Omega multimode microplate reader.

4.9. UV-Ozone Treatment

The mechanical properties of the nanocomposites used in the magnetic hyperthermia biofilm treatment were compared to the mechanical properties of nanocomposites that were exposed to UV-ozone treatment. The MPE-NC films were exposed to UV-ozone for 30 min using a Novascan PSDP-UV8T UV ozone system.

Supporting Information

Supporting Information is available from the Wiley Online Library or from the authors.

Acknowledgements: S.F.S. and J.C. contributed equally to this work. This work was supported by an NSF-CAREER Grant (DMR-1253358) from the NSF Solid State and Materials Chemistry Program.

Received: May 25, 2016; Revised: August 9, 2016; Published online: ; DOI: 10.1002/mame.201600249

Keywords: biofilm eradication; magnetic hyperthermia; magnetic nanocomposites; mechanical properties enhancement; reactive extrusion processing

[1] J. Mansouri, S. Harrisson, V. Chen, *J. Mater. Chem.* **2010**, *20*, 4567.
[2] K. Yoon, K. Kim, X. F. Wang, D. F. Fang, B. S. Hsiao, B. Chu, *Polymer* **2006**, *47*, 2434.
[3] R. P. Schwarzenbach, B. I. Escher, K. Fenner, T. B. Hofstetter, C. A. Johnson, U. von Gunten, B. Wehrli, *Science* **2006**, *313*, 1072.
[4] M. J. Lehtola, M. Laxander, I. T. Miettinen, A. Hirvonen, T. Vartiainen, P. J. Martikainen, *Water Res.* **2006**, *40*, 2151.
[5] D. van der Kooij, H. R. Veenendaal, W. J. Scheffer, *Water Res.* **2005**, *39*, 2789.
[6] W. H. Nicol, (Polyethylene Air Filter), US2612966 A, **1952**.
[7] D. B. Pall, (Portable Unit For Potable Water), US3327859 A, **1967**.
[8] H. J. VanderBilt, T. D. Modert, (Water Filtration), US4753728 A, **1988**.
[9] H. Nagaoka, S. Yamanishi, A. Miya, *Water Sci. Technol.* **1998**, *38*, 497.
[10] J. R. Pan, Y.-C. Su, C. Huang, H.-C. Lee, *J. Membr. Sci* **2010**, *349*, 287.
[11] R. Komlenic, *Filtr. Sep.* **2010**, *47*, 26.
[12] J. Wingender, H. C. Flemming, *Int. J. Hyg. Environ. Health* **2011**, *214*, 417.
[13] S. Wang, G. Guillen, E. M. Hoek, *Environ. Sci. Technol.* **2005**, *39*, 6461.
[14] C. M. Pang, P. Hong, H. Guo, W. T. Liu, *Environ. Sci. Technol.* **2005**, *39*, 7541.
[15] A. Sivan, M. Szanto, V. Pavlov, *Appl. Microbiol. Biotechnol.* **2006**, *72*, 346.
[16] A. Bridier, R. Briandet, V. Thomas, F. Dubois-Brissonnet, *Biofouling* **2011**, *27*, 1017.
[17] T. R. Garrett, M. Bhakoo, Z. B. Zhang, *Prog. Nat. Sci.* **2008**, *18*, 1049.
[18] M. Simoes, L. C. Simoes, M. J. Vieira, *Food Sci. Technol.* **2010**, *43*, 573.
[19] P. Le-Clech, E. K. Lee, V. Chen, *Water Res.* **2006**, *40*, 323.
[20] E. M. Hoek, M. Elimelech, *Environ. Sci. Technol.* **2003**, *37*, 5581.
[21] T. Nguyen, F. A. Roddick, L. Fan, *Membranes* **2012**, *2*, 804.
[22] D. G. Korich, J. R. Mead, M. S. Madore, N. A. Sinclair, C. R. Sterling, *Appl. Environ. Microbiol.* **1990**, *56*, 1423.
[23] I. Mathieson, R. H. Bradley, *Int. J. Adhes. Adhes.* **1996**, *16*, 29.
[24] D. Rodrigues, M. Banobre-Lopez, B. Espina, J. Rivas, J. Azeredo, *Biofouling* **2013**, *29*, 1225.
[25] M. H. Kim, I. Yamayoshi, S. Mathew, H. Lin, J. Nayfach, S. I. Simon, *Ann. Biomed. Eng.* **2013**, *41*, 598.
[26] H. Park, H. J. Park, J. A. Kim, S. H. Lee, J. H. Kim, J. Yoon, T. H. Park, *J. Microbiol. Methods* **2011**, *84*, 41.
[27] J. Stabik, A. Dybowska, J. Pluszyński, M. Szczepanik, Ł. Suchoń, *Adv. Mater. Sci. Eng.* **2010**, *41*, 13.
[28] A. Grujic, N. Talijan, D. Stojanovic, J. Stajic-Trosic, Z. Burzic, L. Balanovic, R. Aleksic, *J. Min. Metall., Sect. B* **2010**, *46*, 25.
[29] S. R. Mishra, M. D. Dickey, O. D. Velev, J. B. Tracy, *Nanoscale* **2016**, *8*, 1309.
[30] C. Galindo-Gonzales, S. Gantz, L. Ourry, F. Mammeri, S. Ammar-Merah, A. Ponton, *Macromolecules.* **2014**, *47*, 3136.
[31] S. Y. Fu, X. Q. Feng, B. Lauke, Y. W. Mai, *Compos. Part B* **2008**, *39*, 933.

[32] X.-Z. Tang, B. Yu, R. V. Hansen, X. Chen, X. Hu, J. Yang, *Adv. Mater. Interfaces* **2015**, *2*, 1500122.
[33] J. Y. Park, S. Kwon, J. H. Kim, *Adv. Mater. Interfaces* **2014**, *1*, 1300089.
[34] T. J. Keener, R. K. Stuart, T. K. Brown, *Compos. Part A* **2004**, *35*, 357.
[35] J. Z. Lu, Q. L. Wu, I. I. Negulescu, *J. Appl. Polym. Sci.* **2005**, *96*, 93.
[36] H. Q. Hong, H. Y. Liao, H. Y. Zhang, H. He, T. Liu, D. M. Jia, *Compos. Part A* **2014**, *64*, 90.
[37] G.-H. Hu, H. Cartier, *Macromolecules*. **1999**, *32*, 4713.
[38] M. Trifkovic, A. T. Hedegaard, M. Sheikhzadeh, S. Huang, C. W. Macosko, *Macromolecules*. **2015**, *48*, 4631.
[39] Y. Yao, E. Metwalli, M. Opel, M. Haese, J.-F. Moulin, K. Rodewald, B. Reiger, P. Mulller-Buschbaum, *Adv. Mater. Interfaces* **2016**, *3*, 1500712.
[40] Y. J. Xie, C. A. S. Hill, Z. F. Xiao, H. Militz, C. Mai, *Compos. Part A* **2010**, *41*, 806.
[41] H. D. Lu, Y. Hu, M. Li, Z. Y. Chen, W. C. Fan, *Compos. Sci. Technol.* **2006**, *66*, 3035.
[42] Z. A. M. Ishak, A. Aminullah, H. Ismail, H. D. Rozman, *J. Appl. Polym. Sci.* **1998**, *68*, 2189.
[43] Z. Zhou, S. F. Wang, L. Lu, Y. X. Zhang, Y. Zhang, *Compos. Sci. Technol.* **2008**, *68*, 1727.
[44] M. Abdelmouleh, S. Boufi, M. N. Belgacem, A. Dufresne, *Compos. Sci. Technol.* **2007**, *67*, 1627.
[45] J. F. Seffer, S. Detriche, J. B. Nagy, J. Delhalle, Z. Mekhalif, *Appl. Surf. Sci.* **2014**, *305*, 301.
[46] W. Wu, Q. G. He, C. Z. Jiang, *Nanoscale Res. Lett.* **2008**, *3*, 397.
[47] M. Yamaura, R. L. Camilo, L. C. Sampaio, M. A. Macedo, M. Nakamura, H. E. Toma, *J. Magn. Magn. Mater.* **2004**, *279*, 210.
[48] D. Maldas, B. V. Kokta, C. Daneault, *J. Appl. Polym. Sci.* **1989**, *37*, 751.
[49] P. J. Herrera-Franco, A. Valadez-González, *Compos. Part B* **2005**, *36*, 597.
[50] P. J. Herrera-Franco, A. Valadez-González, *Compos. Part A* **2004**, *35*, 339.
[51] A. Valadez-Gonzalez, J. M. Cervantes-Uc, R. Olayo, P. J. Herrera-Franco, *Compos. Part B* **1999**, *30*, 309.
[52] B. V. Kokta, R. Chen, C. Daneault, J. L. Valade, *Polym. Compos.* **1983**, *4*, 229.
[53] J. D. Miller, H. Ishida, F. H. J. Maurer, *Rheol. Acta*. **1988**, *27*, 397.
[54] Y. T. Shieh, T. H. Tsai, *J. Appl. Polym. Sci.* **1998**, *69*, 255.
[55] Y. T. Shieh, C. M. Liu, *J. Appl. Polym. Sci.* **1999**, *74*, 3404.
[56] J. F. Arenas, J. I. Marcos, J. C. Otero, I. L. Tocon, J. Soto, *Int. J. Quantum. Chem.* **2001**, *84*, 241.
[57] J. Park, K. An, Y. Hwang, J.-G. Park, H.-J. Noh, J.-Y. Kim, J.-H. Park, N.-M. Hwang, T. Hyeon, *Nat. Mater.* **2004**, *3*, 891.
[58] M. H. Pablico-Lansigan, S. F. Situ, A. C. Samia, *Nanoscale* **2013**, *5*, 4040.
[59] S. F. Situ, A. C. Samia, *ACS Appl. Mater. Interfaces* **2014**, *6*, 20154.
[60] D. J. Burke, N. Pietrasiak, S. F. Situ, E. C. Abenojar, M. Porche, P. Kraj, Y. Lakliang, A. C. Samia, *Int. J. Mol. Sci.* **2015**, *16*, 23630.
[61] L. M. Bauer, S. F. Situ, M. A. Griswold, A. C. Samia, *J. Phys. Chem. Lett.* **2015**, *6*, 2509.
[62] B. D. Cullity, C. D. Graham, *Introduction to Magnetic Materials*, 2nd ed., IEEE Press, Wiley, Hoboken, New Jersey **2009**.
[63] M. Celina, G. A. George, *Polym. Degrad. Stab.* **1995**, *48*, 297.
[64] A. W. Lee, J. P. Santerre, E. Boynton, *Biomaterials* **2000**, *21*, 851.
[65] M. Rocha, A. Mansur, H. Mansur, *Materials* **2009**, *2*, 562.
[66] E. Oral, A. S. Malhi, K. K. Wannomae, O. K. Muratoglu, *J Arthroplasty* **2008**, *7*, 1037.
[67] F. Beckert, S. Bodendorfer, W. Zhang, R. Thomann, R. Mülhaupt, *Macromolecules*. **2014**, *47*, 7036.
[68] D. Intrieri, P. Zardi, A. Caselli, E. Gallo, *Chem. Commun.* **2014**, *50*, 11440.
[69] J.-H. Lee, Y.-M. Huh, Y.-W. Jun, J.-W. Seo, J.-T. Jang, H.-T. Song, S. Kim, E.-J. Cho, H.-G. Yoon, J.-S. Suh, J. Cheon, *Nat. Med.* **2007**, *13*, 95.
[70] S.-H. Noh, W. Na, J.-T. Jang, J.-H. Lee, E. J. Lee, S. H. Moon, Y. Lim, J.-S. Shin, J. Cheon, *Nano Lett.* **2012**, *12*, 3716.
[71] R. A. Chmielewski, J. F. Frank, *J. Food Prot.* **2004**, *67*, 2712.
[72] C. B. Jaquette, L. R. Beuchat, B. E. Mahon, *Appl. Environ. Microbiol.* **1996**, *62*, 2212.
[73] J. Lee, G. Kaletunc, *Appl. Environ. Microbiol.* **2002**, *68*, 5379.
[74] J. Lee, G. Kaletunc, *J. Appl. Microbiol.* **2002**, *93*, 178.
[75] H. Y. Liu, T. L. Doane, Y. Cheng, F. Lu, S. Srinivasan, J. J. Zhu, C. Burda, *Part. Part. Syst. Charact.* **2015**, *32*, 197.
[76] B. Duncan, X. Li, R. F. Landis, S. T. Kim, A. Gupta, L. S. Wang, R. Ramanathan, R. Tang, J. A. Boerth, V. M. Rotello, *ACS Nano* **2015**, *9*, 7775.